Shape coexistence in ^{132}Ba

E. S. Paul, D. B. Fossan, Y. Liang, R. Ma, and N. Xu
Department of Physics, State University of New York at Stony Brook, Stony Brook, New York 11794
(Received 15 May 1989)

Rotational states have been populated in γ-soft ^{132}Ba following the ^{122}Sn(^{13}C,$3n\gamma$) reaction. The ground state of this nucleus is predicted to possess maximal triaxiality $\gamma \sim -30°$. Two $\Delta I = 2$ bands were established, based on quasineutron configurations with large negative γ deformations close to the collective oblate shape $\gamma = -60°$. The bandhead of one of these bands, associated with a $[\nu h_{11/2}]^2$ configuration, was found to be isomeric with a mean lifetime $\tau = 12.5 \pm 0.3$ ns. A third $\Delta I = 2$ band was observed, built on a two-quasiproton configuration with a near-prolate shape ($\gamma \sim 0°$). In addition, two $\Delta I = 1$ bands, built on mixed proton-neutron four-quasiparticle configurations with oblate shapes ($\gamma \sim -60°$), were established.

I. INTRODUCTION

Recent nuclear structure calculations predict[1,2] triaxial shapes for nuclei in the light rare-earth region ($A \sim 130$) together with a softness[3,4] with respect to the shape asymmetry parameter γ. Below the neutron shell closure at $N = 82$, the onset of stable prolate quadrupole deformation ($\gamma \sim 0°$, $\varepsilon_2 \geq 0.2$) occurs for $N \leq 74$ isotones. However, for neutron numbers $76 \leq N \leq 80$, significant triaxial shapes ($\gamma \sim -30°$) are predicted for the nuclear ground states.

For triaxial nuclei with shallow energy potentials with respect to the γ deformation, i.e., γ-soft nuclei, the excitation of quasiparticles in high-j orbitals can greatly influence the nuclear shape.[5,6] Specifically for nuclei in this mass region, the rotational alignment of pairs of protons from the lower $h_{11/2}$ midshell drives the nucleus to a near-prolate ($\gamma \sim 0°$) shape. In contrast, the rotational alignment of pairs of $h_{11/2}$ neutrons from the upper midshell drives the nucleus to a shape near $\gamma = -60°$ which, in the Lund convention,[7] represents the collective rotation of an oblate nucleus about an axis perpendicular to the symmetry axis. Thus the excitation of specific proton or neutron pairs can give rise to shape coexistence in the γ-soft nuclei of the mass $A \sim 130$ region.

Competition between such proton and neutron $[h_{11/2}]^2$ alignments has been observed in nuclei of this mass region. For example, Xe ($Z = 54$) isotopes[8-10] and Ba ($Z = 56$) isotopes[11-15] generally exhibit two S bands corresponding to rotationally aligned $[h_{11/2}]^2$ proton and $[h_{11/2}]^2$ neutron configurations, respectively. Similarly, several $N = 76$ and 78 isotones[16-18] are found to exhibit two S bands, again built on aligned proton and neutron states. These two S bands are predicted[19] to correspond to prolate and oblate nuclear shapes.

High-spin states of the $N = 76$ ^{134}Ce, ^{136}Nd, ^{138}Sm, and ^{140}Gd isotones have recently been studied at Stony Brook. For the heavier nuclei, the proton alignment is favored over the neutron alignment, which has been confirmed by g-factor measurements[20,21] for ^{136}Nd and ^{138}Sm. In contrast, no evidence for proton alignment has thus far been observed in the lighter ^{134}Ce isotone. Indeed, g-factor measurements[22] have indicated only neutron alignment. The present study extends the $N = 76$ systematics to the lighter ^{132}Ba isotone. The results are compared to other $N = 76$ isotones and a comparison is made with cranked shell-model[23] (CSM) calculations for these nuclei.

In-beam spectroscopic studies of ^{132}Ba have previously been reported by both Gizon *et al.*[24] and Flaum *et al.*[25,26] using the ^{124}Sn(^{12}C,$4n\gamma$) reaction, and by Kusakari *et al.*[27] using the ^{133}Cs(p,$2n\gamma$) reaction. Recently, Dewald *et al.*[28] have measured the lifetime of the yrast 10^+ isomer in ^{132}Ba.

II. EXPERIMENTAL METHODS

States in ^{132}Ba were populated via the ^{122}Sn(^{13}C,$3n\gamma$) reaction at a bombarding energy of 57 MeV. The tin target consisted of 10 mg/cm^2 of isotopically enriched ^{122}Sn rolled onto a natural lead backing of thickness 100 mg/cm^2 which served to stop the beam particles. The recoiling nuclei were stopped in the target material largely prior to γ emission, thus minimizing Doppler effects; energy resolutions of 2.0–2.5 keV for the γ-ray transitions were obtained. The ^{13}C beam was provided by the Stony Brook FN tandem van de Graaff accelerator with typical intensities of 1 pnA on target.

An array of five n-type Ge detectors was used to record γ-γ coincidence data. Each Ge detector (efficiency $\sim 25\%$) was surrounded by a bismuth germanate (BGO) anti-Compton shield of the transverse type.[29] Multiplicity information was recorded using 14 hexagonal BGO crystals covering a solid angle in excess of 80% of 4π. In order to reduce background activity and Coulomb excitation lines, only events in which two or more Ge detectors fired in coincidence with at least three of the multiplicity BGO crystals were recorded onto magnetic tape for subsequent off-line analysis.

Approximately 60 million valid coincidence events were written event by event onto magnetic tape. The tapes were scanned off line on a MICROVAX II computer to produce a symmetrized array of E_γ vs E_γ. The background, arising from many weak unresolved continuum γ rays and from Compton scattering of the strong

discrete lines, was subtracted channel by channel from this array using the method outlined in Ref. 30. Gated spectra generated from this background-subtracted array were used to construct the decay scheme of ^{132}Ba presented in Fig. 1. Examples of gated coincidence spectra are shown in Fig. 2.

A subsequent angular distribution experiment was performed for the transitions in ^{132}Ba. One Compton suppressed Ge detector, 22 cm from the target, was positioned sequentially at angles 90°, 115°, 125°, 135°, and 145° with respect to the beam axis. A second Ge detector at −90° served as a monitor. The empirical γ-ray intensities were fitted to the formula

$$W(\theta)=A_0+A_2P_2(\cos\theta)+A_4P_4(\cos\theta)\ , \qquad (1)$$

where θ is the detector angle, $P_2(\cos\theta)$ and $P_4(\cos\theta)$ are Legendre polynomials, while A_0, A_2, and A_4 are adjustable parameters. The results of this analysis are presented in Table I, where a small correction has been made to each A_2/A_0 and A_4/A_0 value to account for the finite size of the detector. For other transitions assigned to ^{132}Ba that were weak or formed doublets in the singles spectra, the intensities were obtained from the coincidence data. These values are also shown in Table I.

Since many of the transitions assigned to ^{132}Ba were only weakly observed in singles spectra, thus precluding definitive angular distribution measurements, an angular correlation analysis was performed making use of the coincidence data. For recording the coincidence data, the Ge detectors, 14.2 cm distant from the target, had been placed at angles of +145°, +78°, +12°, −78°, and −145° with respect to the beam direction. The two detectors close to 90° (+78° and −78°) were sorted against the other three detectors to produce a two-dimensional angular correlation array, from which it was possible to extract average directional correlation[31] (DCO) intensity ratios. Gates were set on known quadrupole transitions along both axes of the correlation array. The intensity ratios of other transitions observed in the two spectra obtained for each gating transition were used to distinguish between dipole and quadrupole transitions. The empirical intensity ratios extracted for quadrupole transitions in this and neighboring nuclei were typically ≥ 1.0, while values ≤ 0.7 were obtained for pure stretched dipole transitions, and values ≤ 0.5 were obtained for known inband $M1/E2$ transitions with negative $E2/M1$ mixing ratios ($\delta<0$). The results of the angular correlation analysis, averaged for several gating quadrupole transitions, are included in Table I.

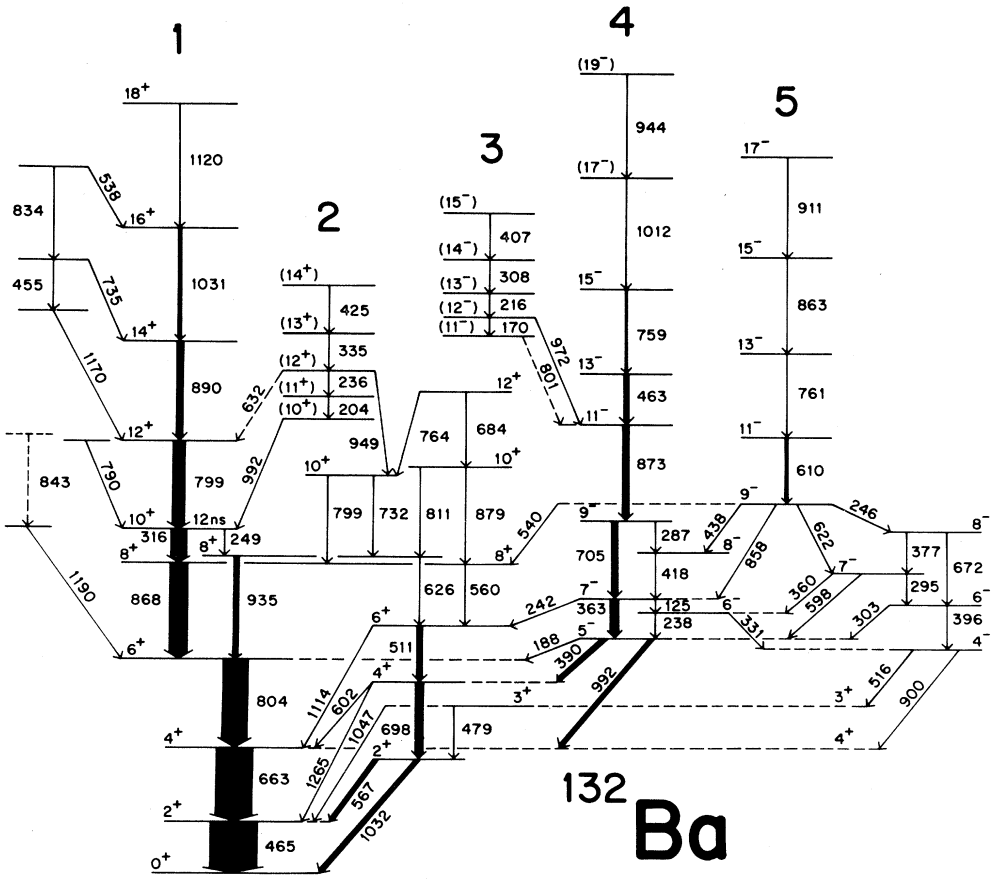

FIG. 1. The decay scheme of ^{132}Ba deduced from this work. The transition energies are given in keV and the widths of the arrows indicate their relative intensities. The yrast 10^+ state of band 1 was found to be isomeric with a mean lifetime $\tau=12.5\pm0.3$ ns.

In order to search for isomeric transitions in ^{132}Ba, a pulsed-beam timing experiment was performed. A 63-MeV ^{12}C beam, accelerated by the Stony Brook tandem, was used to bombard a ^{124}Sn target of thickness 3.5 mg/cm^2 backed by 100 mg/cm^2 of natural lead, producing states in ^{132}Ba via the $4n$ evaporation channel. The natural frequency of the Stony Brook LINAC (not used to accelerate the beam for this experiment) was used to pulse the beam every 106 ns. The distribution of time delays between the arrival of the beam and the detection of the γ rays was recorded event by event onto magnetic tape using a coaxial Ge(Li) detector. The data tapes were sorted off line into a 2048×512 array of E_γ vs t.

III. RESULTS

The decay scheme of ^{132}Ba, deduced from the present study, is shown in Fig. 1 where the rotational bands have been labeled 1–5 in order to facilitate the discussion. The placement of the γ rays in the level scheme was based on coincidence relations and relative intensities. The spin-parity assignments were deduced from the angular distribution and correlation analysis, together with observed decay patterns.

The ground-state band of ^{132}Ba was observed up to $I^\pi=8^+$. The yrast 10^+ state at an excitation energy of 3116 keV (part of band 1) was found to be isomeric with a mean lifetime of $\tau=12.5\pm0.3$ ns. This average value, obtained from the decay curves of the 465-, 663-, 804-, 868-, and 316-keV transitions, is slightly longer than the value $\tau=10.8\pm0.9$ ns recently reported by Dewald *et al.*[28] The yrast band 1 could be followed up to $I^\pi=18^+$.

Several other positive-parity states were populated in ^{132}Ba, including the 2^+, 3^+, 4^+, and 6^+ members of the γ-vibrational band. The 2^+ bandhead of the γ-vibrational band, at an excitation energy of 1032 keV, lies below the yrast 4^+ level at 1128 keV; similar low-lying γ-vibrational bandheads have been observed in other $N=76$ isotones ranging from Te to Gd ($52\le Z\le64$).

A γ ray of energy 798.9 keV feeds the yrast 8^+ level. This transition forms a doublet with the 799.5-keV $12^+\rightarrow10^+$ yrast transition of band 1. However, the 798.9-keV transition could be distinguished by gating on the 949- and 764-keV transitions placed above this γ ray in the decay scheme. A coincidence gate, set on the 949-keV transition, is shown in Fig. 2(c). A third 10^+ state was established at an energy of 3679 keV.

The 5^-, 6^-, 7^-, and 8^- states shown at the bottom of

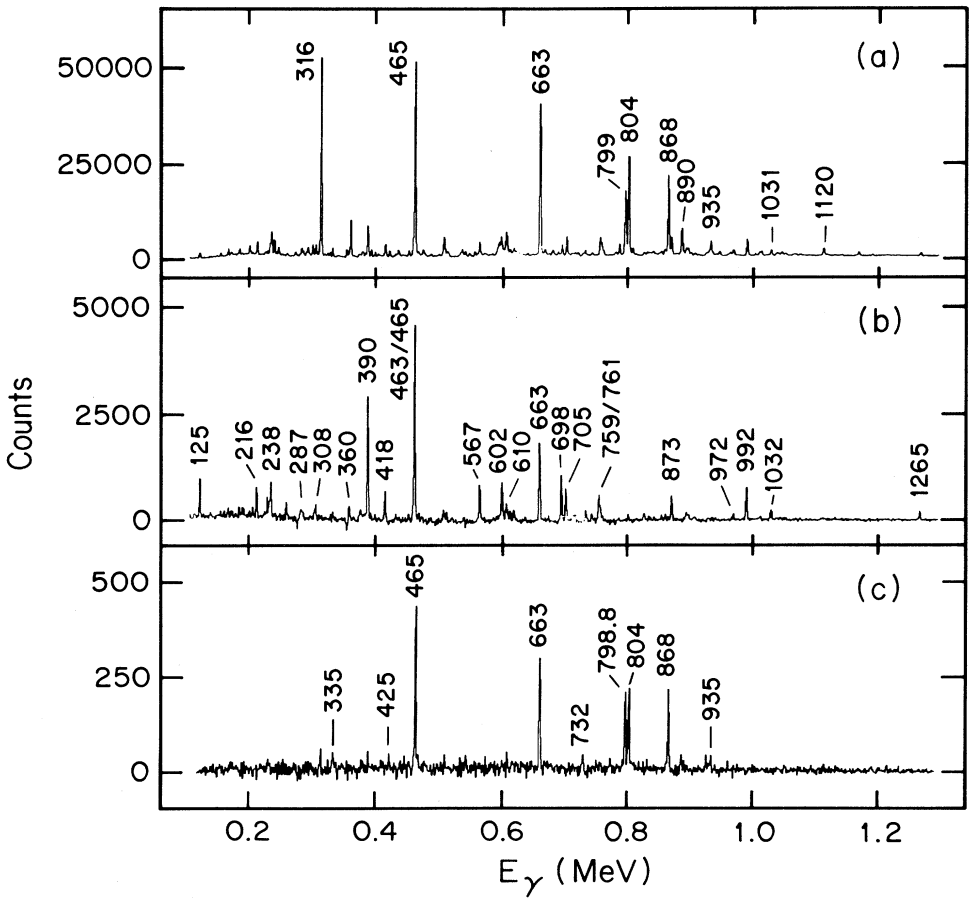

FIG. 2. Examples of gated coincidence spectra. The transition energies are labeled in keV. (a) A sum of gates set on the 465-, 663-, 804-, and 868-keV transitions of the ground-state band. (b) A sum of gates set on the 125- and 238-keV transitions near the bottom of band 4. (c) A gate set on the 949-keV transition showing the 798.8-keV ($10^+\rightarrow8^+$) transition.

TABLE I. Energies, intensities, and angular distribution data for the transitions assigned to ^{132}Ba following the ^{122}Sn(^{13}C,3$n\gamma$) reaction at 57 MeV.

E_γ[a] keV	Rel.[b] intensity	A_2/A_0	A_4/A_0	DCO[c] ratio	Mult.	Assignment
125.5	2.5(0.3)[d]	−0.508(42)	+0.140(64)	0.43(07)	$M1/E2$	$7^-\rightarrow6^-$
169.7	0.9(0.2)			1.0(2)		
187.7	0.9(0.2)			0.64(10)	$E1$	$5^-\rightarrow6^+$
203.8	1.0(0.2)			0.5(1)	$(M1/E2)$	$(11^+\rightarrow10^+)$
215.6	2.9(0.1)			0.59(06)	$(M1/E2)$	$(13^-\rightarrow12^-)$
235.7	1.0(0.3)			0.5(1)	$(M1/E2)$	$(12^+\rightarrow11^+)$
237.9	4.7(0.2)[d]	−0.726(77)	+0.24(11)	0.42(02)	$M1/E2$	$6^-\rightarrow5^-$
242.4	4.5(0.2)	−0.434(73)	+0.09(10)	0.61(04)	$E1$	$7^-\rightarrow6^+$
245.6	<1.0					$9^-\rightarrow8^-$
249.1	1.4(0.1)			0.93(11)	$E2$	$10^+\rightarrow8^+$
285.6	2.7(0.2)			0.67(05)	Dipole	$\rightarrow4^-$
287.5	1.5(0.2)			0.47(07)	$M1/E2$	$9^-\rightarrow8^-$
295.1	2.0(0.2)	−0.62(10)	+0.08(13)	0.39(04)	$M1/E2$	$7^-\rightarrow6^-$
303.2	2.7(0.2)	−0.807(66)	+0.084(94)	0.23(04)	$M1/E2$	$6^-\rightarrow5^-$
307.9	2.6(0.1)	−0.38(10)	−0.07(13)	0.65(07)	$M1/E2$	$(14^-\rightarrow13^-)$
315.9	29.0(0.3)	+0.185(52)[e]	−0.021(64)[e]	1.05(02)	$E2$	$10^+\rightarrow8^+$
330.8	1.1(0.1)					$6^-\rightarrow4^-$
335.0	1.2(0.2)			0.4(1)	$(M1/E2)$	$(13^+\rightarrow12^+)$
360.5	<1.0					$7^-\rightarrow6^-$
363.5	15.5(0.2)	+0.049(52)[e]	+0.005(67)[e]	1.07(04)	$E2$	$7^-\rightarrow5^-$
377	1.3(0.2)	−0.590(65)	+0.027(91)	0.28(04)	$M1/E2$	$8^-\rightarrow7^-$
390.2	15.9(0.3)[d]	−0.213(50)	−0.050(63)	0.70(05)	$E1$	$5^-\rightarrow4^+$
395.7	2.2(0.2)			1.20(16)	$E2$	$6^-\rightarrow4^-$
407	1.0(0.1)			0.68(13)	$(M1/E2)$	$(15^-\rightarrow14^-)$
417.5	4.9(0.2)	f	f	0.30(02)	$M1/E2$	$8^-\rightarrow7^-$
424.5	1.1(0.2)			0.5(1)	$(M1/E2)$	$(14^+\rightarrow13^+)$
438.4	1.8(0.2)			0.77(11)	$M1/E2$	$9^-\rightarrow8^-$
454.7	1.8(0.2)			0.57(17)	Dipole	
463	≡100[d]	+0.244(54)	−0.026(63)	0.98(05)	$E2$	$13^-\rightarrow11^-$
464.6				1.06(02)	$E2$	$2^+\rightarrow0^+$
479.3	4.8(0.2)[d]	+0.15(10)	+0.01(12)	0.98(09)	$M1/E2$	$3^+\rightarrow2^+$
511.5	8.8(0.2)			0.89(06)	$E2$	$6^+\rightarrow4^+$
516.0	3.8(0.2)			0.54(08)	$E1$	$4^-\rightarrow3^+$
537.5	2.1(0.2)	−0.10(18)	≡0.0	0.42(09)	$(M1/E2)$	$\rightarrow16^+$
539.8					$(E1)$	$9^-\rightarrow8^+$
559.6	1.8(1)			0.77(16)	$E2$	$8^+\rightarrow6^+$
567.4	11.2(0.2)[d]	−0.026(64)	+0.031(83)	0.81(04)	$M1/E2$	$2^+\rightarrow2^+$
598.5	4.2(02)			1.21(07)	$E2$	$7^-\rightarrow5^-$
602.0	3.2(0.2)			0.66(04)	$M1/E2$	$4^+\rightarrow4^+$
610.3	7.6(0.3)	g	g	1.06(07)	$E2$	$11^-\rightarrow9^-$
622.0	2.1(0.2)					$9^-\rightarrow7^-$
626.2	1.9(0.1)	+0.388(75)[g]	+0.020(91)[g]	1.27(20)	$E2$	$8^+\rightarrow6^+$
632	<1.0					$(12^+)\rightarrow12^+$
663.4	75.9(1.2)[d]	+0.315(54)	−0.028(63)	1.02(02)	$E2$	$4^+\rightarrow2^+$
672.0	0.9(0.1)			1.22(16)	$E2$	$8^-\rightarrow6^-$
683.9	1.7(0.2)	+0.242(56)	−0.049(67)	1.7(6)	$E2$	$12^+\rightarrow10^+$
697.9	8.3(0.2)	+0.206(61)[g]	−0.016(73)[g]	1.16(07)	$E2$	$4^+\rightarrow2^+$
705.2	12.3(0.5)[d]	+0.305(58)	−0.017(69)	1.08(06)	$E2$	$9^-\rightarrow7^-$
731.5	0.8(0.1)			1.00(22)	$E2$	$10^+\rightarrow8^+$
734.9	1.6(0.2)			0.34(10)	$M1/E2$	$\rightarrow14^+$
758.5	7.5(0.2)[d]	+0.378(74)	−0.088(89)	1.12(06)	$E2$	$15^-\rightarrow13^-$
761.0	3.8(0.4)			1.25(15)	$E2$	$13^-\rightarrow11^-$
763.5	3.1(0.3)			1.05(13)	$E2$	$12^+\rightarrow10^+$
789.9	2.6(0.2)	−0.804(78)[g]	+0.11(11)[g]	0.18(03)	$M1/E2$	$\rightarrow10^+$
798.8	22.8(0.4)[d]	+0.249(57)	−0.083(68)	0.94(02)	$E2$	$10^+\rightarrow8^+$
799.5					$E2$	$12^+\rightarrow10^+$
801	<1.0					
804.5	53.6(0.9)[d]	+0.301(54)	−0.031(64)	1.01(02)	$E2$	$6^+\rightarrow4^+$

TABLE I. (*Continued*).

E_γ[a] keV	Rel.[b] intensity	A_2/A_0	A_4/A_0	DCO[c] ratio	Mult.	Assignment
811.0	1.7(0.2)			0.93(12)	$E2$	$10^+\rightarrow 8^+$
834	<1.0					
843	<1.0					
857.6	1.6(0.1)	+0.57(14)	≡0.0	1.01(16)	$E2$	$9^-\rightarrow 7^-$
862.5	2.5(0.1)			0.90(13)	$E2$	$15^-\rightarrow 13^-$
868.4	33.1(0.6)[d]	+0.323(56)	−0.032(65)	1.07(02)	$E2$	$8^+\rightarrow 6^+$
873.1	8.6(0.2)[d]	+0.319(71)	+0.017(68)	1.08(06)	$E2$	$11^-\rightarrow 9^-$
879	<1.0				($E2$)	$10^+\rightarrow 8^+$
889.5	9.2(0.2)[d]	+0.378(68)	−0.112(80)	0.96(04)	$E2$	$14^+\rightarrow 12^+$
899.5	3.4(0.1)	+0.269(58)[g]	−0.049(69)[g]	0.62(08)	$E1$	$4^-\rightarrow 4^+$
910.8	0.9(0.1)			1.1(4)	$E2$	$17^-\rightarrow 15^-$
935.0	8.4(0.4)[d]	+0.37(10)	−0.22(12)	1.08(06)	$E2$	$8^+\rightarrow 6^+$
944.0	2.2(0.3)			1.07(22)	$E2$	$(19^-\rightarrow 17^-)$
949	1.8(0.2)			1.04(12)	$E2$	$12^+\rightarrow 10^+$
971.7	3.9(0.2)	−0.062(68)	−0.054(88)	0.79(09)	Dipole	$\rightarrow 11^-$
992	14.1(0.3)[d]	−0.218(55)	−0.010(75)			$(10^+)\rightarrow 10^+$
992.4				0.61(03)	$E1$	$5^-\rightarrow 4^+$
1012.0	3.3(0.3)			0.92(15)	($E2$)	$(17^-)\rightarrow 15^-$
1030.5	5.5(0.2)[d]	+0.138(84)	+0.03(11)	1.08(11)	$E2$	$16^+\rightarrow 14^+$
1032.0				1.4(2)	$E2$	$2^+\rightarrow 0^+$
1046.7	3.4(0.3)[d]	+0.107(70)	−0.025(88)	1.04(10)	$M1/E2$	$3^+\rightarrow 2^+$
1113.5	5.9(0.1)	f	f	0.98(07)	$E2$	$6^+\rightarrow 4^+$
1120	4.4(0.2)[d]	+0.252(67)	≡0.0		$E2$	$18^+\rightarrow 16^+$
1169.5	1.6(0.2)			0.76(09)	Dipole	$\rightarrow 12^+$
1190.4	0.7(0.1)			1.0(3)		$\rightarrow 6^+$
1265.3	4.2(0.2)[d]	+0.36(10)	−0.04(12)	1.04(09)	$E2$	$4^+\rightarrow 2^+$

[a]Transition energies are accurate to ±0.2 keV except those values quoted as integers which are accurate to ±1 keV.
[b]Except where stated, the transition intensities were obtained from the coincidence data.
[c]Angular correlation ratios are average values obtained from several gating quadrupole transitions.
[d]Intensity obtained from the angular distribution data.
[e]Value perturbed by a dipole transition in ^{131}Ba.
[f]Doublet with a strong dipole in ^{131}Ba.
[g]Doublet with a transition in ^{131}Ba.

band 4 in Fig. 1 have previously been reported by Gizon *et al.*[24] Two transitions of energies 992 and 390 keV depopulate the 5^- level, feeding into the 4^+ members of the ground-state band and γ-vibrational band, respectively. The angular distribution and correlation data for these two transitions are consistent with the pure stretched dipole ($E1$) assignments. The angular distribution results obtained for the 238-keV ($6^-\rightarrow 5^-$) and 125-keV ($7^-\rightarrow 6^-$) dipole transitions imply mixed $M1/E2$ character with an $E2/M1$ mixing ratio $\delta\sim -0.2$. From the present data, the next dipole transition of energy 418 keV ($8^-\rightarrow 7^-$) is contaminated with a strong dipole transition of ^{131}Ba; thus reliable angular distribution could not be obtained for this transition. However, the angular correlation data for this and the next (287 keV) dipole suggest mixed $E2/M1$ character similar to the 238- and 125-keV transitions. No transition was observed between the 8^- and 6^- states. From the measured branching ratios of the quadrupole and dipole transitions depopulating the 9^- and 7^- states, it is possible to extract an average value of ~ 0.5 $(\mu_N/eb)^2$ for the ratios of reduced transition probabilities $B(M1;\Delta I=1)/B(E2;\Delta I=2)$ for this band. The odd-spin members of this sideband could be followed up through a backbend to $I^\pi=(19^-)$ with reasonable intensity, showing a second backbend at the highest observed spins.

A second $\Delta I=2$ sideband (band 5), built on a 9^- state, was observed up to $I^\pi=17^-$. The 9^- bandhead decays by five transitions into other states of ^{132}Ba. A transition of energy 540 keV feeds the yrast 8^+ level; two transitions of energies 438 and 858 keV feed the lower members of band 4; and two transitions of 246 and 622 keV feed another weak band structure shown to the extreme right in Fig. 1.

Two $\Delta I=1$ sidebands were established in ^{132}Ba from the present analysis. One band (band 3), consisting of energies 170, 216, 308, and 407 keV with intensities of $\sim 3\%$ of the $2^+\rightarrow 0^+$ transition, feeds into band 4 via a transition of energy 972 keV. The angular distribution and correlation data suggest this transition to be of dipole character, favoring a mixed $M1/E2$ assignment. This $\Delta I=1$ sideband therefore most likely possesses negative parity.

A second $\Delta I=1$ band (band 2, 204, 236, 335, 425 keV)

of ~1% intensity is weakly connected to the yrast band 1 via a transition of energy 992 keV (a doublet with the strong 992-keV $5^- \rightarrow 4^+$ transition that depopulates band 4), and a second 10^+ state via the 949-keV transition [a gate on this transition is shown in Fig. 2(c)]. The decay pattern suggests that this band has positive parity.

Several other γ rays, feeding the yrast band, are shown to the extreme left in Fig. 1, while several other negative-parity states are shown to the extreme right.

IV. DISCUSSION

The band structures of ^{132}Ba are first discussed; secondly, results for several $N=76$ isotones are compared to theory providing evidence for significant triaxial shapes for these nuclei at low spins.

A. The yrast band

Recent potential energy surface (PES) calculations,[1] using a triaxially deformed Woods-Saxon single-particle potential, have predicted the ground state of ^{132}Ba to be near prolate ($\varepsilon_2=0.14$, $\gamma=-2°$). In contrast, recent total Routhian surface (TRS) cranking calculations[2] based on a universal Woods-Saxon potential[32] and treating the deformation parameters self-consistently predict a triaxial minimum ($\varepsilon_2=0.15$, $\gamma\sim-30°$) for ^{132}Ba at low spins. However, both calculations predict soft energy potentials with respect to the γ deformation. The PES calculations predict an oblate-prolate energy difference less than 300 keV, while for the TRS calculations the axially symmetric prolate and oblate shapes ($\gamma=0°$ and $-60°$, respectively) are predicted to lie less than 200 keV above the triaxial $\gamma\sim-30°$ minimum. The TRS calculations show the triaxial minimum for rotational frequencies $\hbar\omega<0.25$ MeV, corresponding to the ground-state rotational band of ^{132}Ba.

For light barium nuclei, CSM calculations predict low-frequency rotational alignments of both $h_{11/2}$ proton and neutron pairs. Indeed, several barium isotopes[11–15] (^{122}Ba$\rightarrow$ ^{130}Ba) show two S bands associated with aligned $h_{11/2}$ proton and neutron pairs, respectively. For triaxial nuclear shapes ($\gamma<0°$), the neutron alignment is more favored over the proton alignment. Hence, for ^{132}Ba, it is expected that $h_{11/2}$ neutrons will be responsible for the first backbend in the yrast band. Indeed, a recent g-factor measurement[33] has confirmed the $[\nu h_{11/2}]^2$ nature of the yrast 10^+ state of band 1 at 3116 keV.

The excitation of a pair of $h_{11/2}$ quasineutrons introduces a driving force on the nuclear core towards large negative values of γ. Simple CSM calculations using the formalism of Ref. 6 yield values close to $\gamma=-60°$, the axially symmetric collective oblate shape, while the TRS calculations[2,19] predict a minimum to develop at $\gamma\sim-80°$ above a rotational frequency $\hbar\omega=0.3$ MeV. The crossing frequency for the $[\nu h_{11/2}]^2$ alignment in the yrast band, extracted from experimental Routhian plots,[23] is $\hbar\omega_c=0.35$ MeV. The large nuclear shape change ($\gamma\sim-30°$–$-80°$) associated with the alignment of the $h_{11/2}$ neutron pair may explain why the 10^+ bandhead of this two-quasineutron configuration is found to be isomeric.

In addition to the yrast 10^+ state, two further 10^+ states were established in ^{132}Ba. One of these may be associated with a $[\pi h_{11/2}]^2$ two-quasiproton configuration with a near-prolate shape ($\gamma\sim0°$), as seen in the heavier $N=76$ isotones.

B. The $\Delta I=2$ sidebands

Both two-quasineutron and two-quasiproton configurations are possible candidates for bands 4 and 5 in ^{132}Ba. Following studies of lighter barium nuclei by Flaum *et al.*,[25,26] Gizon *et al.*[24] proposed a $\pi h_{11/2}\otimes\pi g_{7/2}$ structure for the lower members of band 4. However, the present analysis favors a two-quasineutron structure for band 4, with band 5 being related to this two-quasiproton structure.

For a prolate ($\gamma=0°$) nuclear shape of modest quadrupole deformation $\varepsilon_2=0.15$, the Nilsson orbitals closest to the Fermi surface are the $[550]\frac{1}{2}^-$ ($\pi h_{11/2}$), $[420]\frac{1}{2}^+$, and $[422]\frac{3}{2}^+$ ($\pi g_{7/2}$ with $\pi d_{5/2}$ admixtures) orbitals. Coupling of the $\pi h_{11/2}$ orbital to either of the positive-parity orbitals in accordance with the Gallagher-Moszkowski rule[34] yields a K value of 1. The two quasiprotons are essentially rotationally aligned and a band built on the $\pi h_{11/2}\otimes\pi g_{7/2}$ configuration would possess a high-spin bandhead (cf. the yrast 10^+ state built on rotationally aligned $h_{11/2}$ neutrons). For this reason, band 5, built on a 9^- state, and not band 4, is associated with the $\pi h_{11/2}\otimes\pi g_{7/2}$ two-quasiproton configuration. CSM calculations of total Routhians[6] predict this proton configuration to possess a shape with $\gamma>0°$, but close to the prolate $\gamma=0°$ shape, which is caused by the strong driving force of the proton from the bottom of the $h_{11/2}$ shell to $\gamma>0°$. The numerous transitions decaying from the 9^- bandhead support the prediction of a vastly different nuclear shape for this two-quasiproton configuration; whereas band 5 possesses a shape $\gamma>0°$, all the other low-lying levels of ^{132}Ba possess shapes with large negative γ deformations $\gamma\ll0°$.

Instead of a two-quasiproton structure, band 4 is associated with a two-quasineutron configuration, possibly a $\nu h_{11/2}\otimes\nu d_{3/2}$ or a $\nu h_{11/2}\otimes\nu s_{1/2}$ configuration. For these configurations, the nuclear shape is dominated by the $h_{11/2}$ neutron which favors a large negative γ deformation close to the collective oblate $\gamma=-60°$ shape, as discussed previously. Thus the lower part of band 4 is probably based on a nuclear shape of large negative γ deformation. Several dipole transitions of energies 238, 125, 418, and 287 keV link the two signatures of this configuration which shows a signature splitting $\Delta e'\sim100$ keV. The $8^-\rightarrow6^-$ transition of the unfavored signature component was not observed. The dipole transitions possess negative $E2/M1$ mixing ratios $\delta\sim-0.2$.

The negative-parity levels shown at the extreme right in Fig. 1 are probably also associated with a similar two-quasineutron configuration. Again, two dipole transitions (295 and 377 keV) with negative $E2/M1$ mixing ratios were observed linking the two signatures.

At the 11^- state, band 4 backbends. The experimental crossing frequency extracted for the backbend is $\hbar\omega=0.31$ MeV. This backbend is attributed to the rota-

tional alignment of a further pair of $h_{11/2}$ neutrons which maintains the nuclear shape at the large negative γ deformation. The fact that this crossing frequency for the second and third valence $h_{11/2}$ neutrons (the "blocked" crossing) is lower than that observed for the first and second ("unblocked") valence $h_{11/2}$ neutrons in the yrast band can be readily explained. First, the large negative γ deformation expected for band 4 reduces the $h_{11/2}$ neutron crossing frequencies (both blocked and unblocked). It is found from CSM calculations that the minimum crossing frequency for a specific quasiparticle pair occurs at the energy minimum in the γ plane predicted for that specific pair. This is illustrated in Fig. 3, where CSM calculations for the ^{136}Nd isotone are presented. The nuclear shape for the lower part of band 4 is maintained at $\gamma \leq -60°$ by the presence of one $h_{11/2}$ quasineutron, which thus minimizes the alignment frequencies for $h_{11/2}$ quasineutrons. However, the $h_{11/2}$ neutron blocks the alignment of the first pair of valence $h_{11/2}$ neutrons. Second, the occupation of two quasineutron orbitals reduces their contributions to the neutron pairing energy Δ_n, again lowering the crossing frequency for $h_{11/2}$ neutrons. Hence, it is not unreasonable that the blocked $[\nu h_{11/2}]^2$ crossing in band 4 ($\gamma \leq -60°$) occurs at a lower frequency than the unblocked crossing in the yrast band ($\gamma \sim -30°$) because of the large difference in the nuclear shape. Indeed, it can be seen in Fig. 3 that the blocked $[\nu h_{11/2}]^2$ alignment (labeled *bc*) for $\gamma \sim -60°$ occurs at a similar frequency to the unblocked alignment (*ab*) for $\gamma \sim -30°$.

To summarize, band 5 is believed to be built on a two-quasiproton configuration with a near-prolate shape. Band 4 is interpreted as built on a two-quasineutron configuration of large negative γ deformation that evolves into a four-quasineutron configuration when a pair of $h_{11/2}$ neutrons align.

C. The $\Delta I=1$ sidebands

Bands 2 and 3 consist of a regular series of dipole transitions, the $E2$ crossover transitions being too weak to observe in the present experiments. These two $\Delta I=1$ bands may be interpreted in terms of high-K two-quasineutron–two-quasiproton configurations of either collective prolate ($\gamma \sim 0°$) or collective oblate ($\gamma \sim -60°$) shapes. For a prolate ($\gamma=0°$) shape low-Ω $h_{11/2}$ protons ($\Omega \sim \frac{1}{2}$) and high-Ω $h_{11/2}$ neutrons are near the Fermi surface. However, for an oblate ($\gamma=-60°$) shape, the roles are reversed; high-Ω $h_{11/2}$ protons ($\Omega \sim \frac{11}{2}$) and low-Ω $h_{11/2}$ neutrons are near the Fermi surface. Such high-Ω orbitals ($h_{11/2}$ neutrons for $\gamma \sim 0°$, $h_{11/2}$ protons for $\gamma \sim -60°$) are required to enhance the $B(M1)$ transition rates within the band. The largest enhancement of the $B(M1)$ rate will occur for a coupled ($\Omega=\frac{11}{2}$) $h_{11/2}$ proton at $\gamma \sim -60°$. The large g factor (~ 1.2) of the $h_{11/2}$ proton leads to a sizable component of the magnetic moment perpendicular to the total spin of the nucleus. The $B(M1)$ rate, proportional to the square of this component, is thus increased.

Experimental $B(M1;\Delta I=1)/B(E2;\Delta I=2)$ ratios for $\nu h_{11/2}$ bands in near-prolate ($\gamma \sim -10°$) odd-N nuclei[35–37] are typically $\sim 1(\mu_N/eb)^2$, while values obtained for $\pi h_{11/2}$ bands in oblate ($\gamma \sim -60°$) odd-Z nuclei[38] are typically an order of magnitude larger. Because of the weakness in the $E2$ crossover transitions in the two $\Delta I=1$ bands in ^{132}Ba, such ratios could not be extracted.

Considering the available orbitals nearest to the Fermi surface for an oblate shape, two possible configurations for the $\Delta I=1$ sidebands are the negative-parity

$$\pi h_{11/2} \otimes \pi g_{7/2} \otimes [\nu h_{11/2}]^2$$

(band 3) and positive-parity

$$\pi h_{11/2} \otimes \pi g_{7/2} \otimes \nu h_{11/2} \otimes \nu d_{3/2}$$

(band 2) configurations at $\gamma \sim -60°$. The dominant feature of these bands is the coupling of the high-j, low-Ω, $h_{11/2}$ neutron and the high-j, high-Ω, $h_{11/2}$ proton.

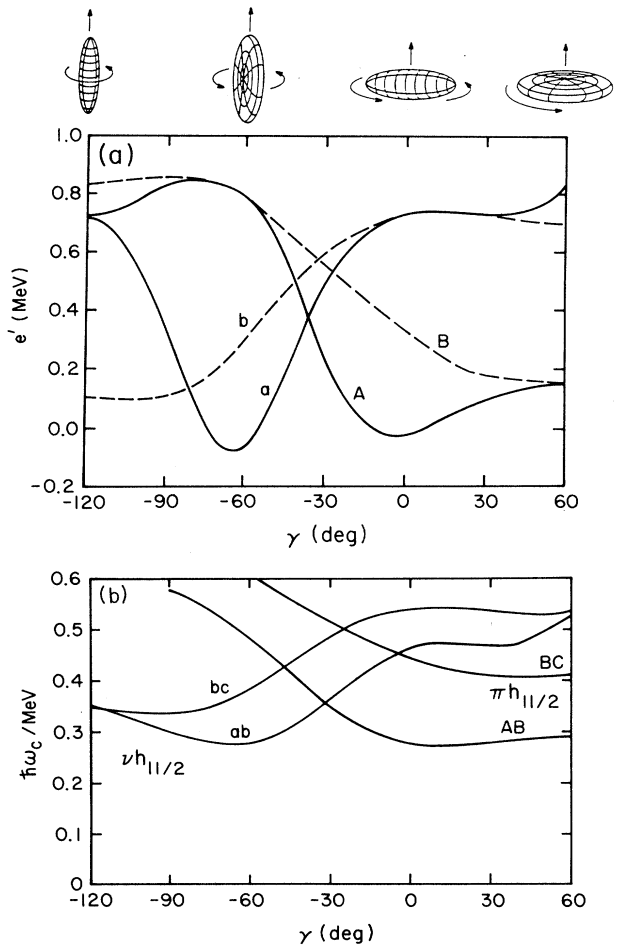

FIG. 3. Proton (A and B) and neutron (a and b) $h_{11/2}$ quasiparticle levels (top) as a function of the γ deformation. Calculated unblocked (AB and ab) and blocked (BC and bc) $h_{11/2}$ proton and neutron crossing frequencies (bottom) as a function of the γ deformation. These CSM calculations were performed specifically for the $N=76$ ^{136}Nd isotone. The shape of the nucleus and sense of rotation is indicated at the top of the figure for specific values of γ that correspond to axially symmetric shapes.

This configuration is expected to show the properties of the $\Delta I=1$ bands, namely enhanced $M1$ transitions linking the two signature components and no energy splitting between the two signature components.

Similar collective oblate rotational bands have been observed in several odd-Z nuclei, including ^{131}La (Ref. 39) and ^{137}Pr (Ref. 40), based on the $\pi h_{11/2}\otimes[\nu h_{11/2}]^2$ configuration. More recently, such bands have been established[41] in doubly odd ^{128,130}La based on related four-quasiparticle configurations that contain $h_{11/2}$ protons and neutrons. The even-even ^{126}Xe nucleus[9] possesses a similar $\Delta I=1$ band that could be of the same origin to those observed in ^{132}Ba.

The most influential orbitals in these bands are the $h_{11/2}$ proton and $h_{11/2}$-neutron quasiparticles. The $h_{11/2}$ neutron drives to large negative γ deformation where the $\Omega=\frac{11}{2}$ component of the $h_{11/2}$ proton is nearest the Fermi surface. This high-Ω $h_{11/2}$ proton orbital is responsible for the enhancement of the $M1$ transitions as described above. The two signatures of the band are obtained by occupying the two signatures of the $\pi h_{11/2}$ orbital, respectively. For an oblate nuclear shape $\gamma\sim-60°$, the two signatures of this high-Ω $\pi h_{11/2}$ orbital are essentially degenerate. Thus, a regular set of dipole transitions (no signature splitting) would be observed, as is the case for these nuclei experimentally. It should be noted that a $[\nu h_{11/2}]^2\otimes[\pi h_{11/2}]^2$ configuration would lead only to a decoupled even-spin rotational band of unique signature since both signature components of the $h_{11/2}$-proton and $h_{11/2}$-neutron orbitals are occupied, respectively.

D. $N=76$ systematics: Further evidence for triaxial shapes

1. γ-vibrational band systematics

In terms of the asymmetric rotor model[42] of Davydov *et al.*, a comparison of the low-lying levels of the ground-state rotational band and γ-vibrational band can provide an insight into the degree of triaxiality possessed by a nucleus. In this formalism, it is possible to extract the magnitude of the γ deformation from the ratio of the 2^+ energies of the ground-state and γ-vibrational bands. Such values of $|\gamma|$ are presented in Table II for $N=76$ isotones[43,27,44] ranging from tellurium to gadolinium ($52\le Z\le 64$). It can be seen that values of $|\gamma|\sim 26°$ are obtained for this series of nuclei consistent with recent TRS calculations[2] which predict γ deformations $-30°\le\gamma\le-25°$ at low spins. For a triaxial rotor of maximal γ deformation, energy minima exist at $\gamma=+30°$, $-30°$, and $-90°$ from symmetry considerations. However, the collective rotation of the nucleus favors the $\gamma=-30°$ minimum where the moment of inertia is largest.

The following relations between energy levels hold in the asymmetric rotor model

$$E_1(2^+)+E_2(2^+)=E(3^+)\,, \tag{2}$$

and

$$4E_1(2^+)+E_2(2^+)=E(5^+)\,. \tag{3}$$

TABLE II. Triaxial rotor model (Ref. 42) analysis for several $N=76$ isotones. The percentage differences R_3 and R_5 are defined as $R_3=[E_1(2^+)+E_2(2^+)-E(3^+)]/[E_1(2^+)+E_2(2^+)]$ (%) and $R_5=[4E_1(2^+)+E_2(2^+)-E(5^+)]/[4E_1(2^+)+E_2(2^+)]$ (%), respectively.

Nucleus	$\lvert\gamma\rvert$ (deg)	R_3 %	R_5 %
$^{128}_{52}$Te	26.6	−1.21	
$^{130}_{54}$Xe	27.6	+1.55	
$^{132}_{56}$Ba	26.3	−0.98	
$^{134}_{58}$Ce	25.3	−1.79	
$^{136}_{60}$Nd	25.7	+0.38	+13.2
$^{138}_{62}$Sm	27.0	+0.79	+18.7
$^{140}_{64}$Gd	26.8	−2.53	+16.5

Table II includes the percentage differences in these relations, R_3 and R_5, as defined in the caption. The R_3 values are of the order of 1% while the R_5 values, where available, are somewhat larger, being typically 15%. It can be seen that the asymmetric rotor model is valid for these nuclei but only at low spins.

2. Proton and neutron crossing frequencies

Similarly to ^{132}Ba, g-factor measurements[22] for ^{134}Ce have indicated a 10^+ state built on a $[\nu h_{11/2}]^2$ configuration. For ^{136}Nd and ^{138}Sm, S bands built on both $[\nu h_{11/2}]^2$ and $[\pi h_{11/2}]^2$ configurations have been established;[16,17] g-factor measurements[20,21] have indicated that the yrast S bands of these heavier isotones are associated with the proton configuration. From this systematic data it is possible to extract quasiparticle alignment frequencies for both $h_{11/2}$-proton and $h_{11/2}$-neutron pairs.

Such experimental $[h_{11/2}]^2$ proton and neutron crossing frequencies are plotted in Fig. 4 for several $N=76$ isotones where they are compared to cranked shell-model predictions. The CSM calculations were performed for prolate ($\gamma=0°$) nuclear shapes using quadrupole ε_2 and hexadecapole ε_4 deformation parameters obtained[45] from potential energy surface calculations using the Nilsson-

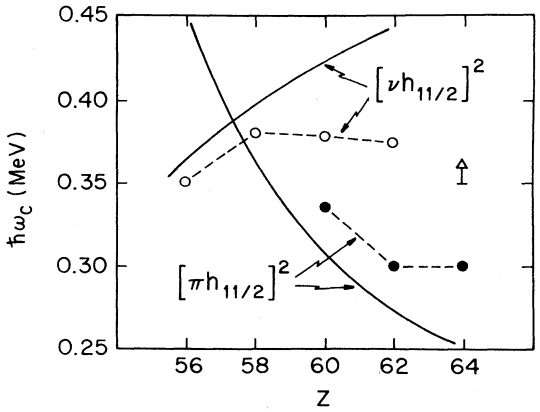

FIG. 4. A comparison of experimental (circles) and theoretical (solid lines) CSM $h_{11/2}$ proton and neutron crossing frequencies for several $N=76$ isotones.

Strutinsky method.[46] The proton and neutron pairing energies were taken as 80% of the odd-even mass differences where possible, and extrapolated values where not possible. For the proton calculations, κ and μ Nilsson parameters fitted[47] to this mass region were used, while values of Ref. 48 were used for the neutrons. The proton and neutron Fermi energies, λ_p and λ_n, were chosen to reproduce the appropriate particle numbers at zero frequency for each nucleus under consideration.

It can be seen from Fig. 4 that the experimental proton crossing frequencies are systematically larger than the predicted values, while the experimental neutron crossing frequencies are systematically smaller, and that the discrepancy increases for the heavier isotones. These observations are consistent with triaxial shapes ($\gamma < 0°$) predicted for the ground-state bands of these nuclei. The triaxial deformation ($\gamma \sim -25°$) hinders the alignment of lower-midshell $h_{11/2}$ protons while favoring the alignment of upper-midshell $h_{11/2}$ neutrons, as illustrated in Fig. 3.

V. SUMMARY

Several rotational bands have been observed in the γ-soft ^{132}Ba nucleus. The ground-state band is predicted to possess maximal triaxiality $\gamma \sim -30°$, and is crossed by a band built on a $[\nu h_{11/2}]^2$ configuration with a large negative γ deformation close to the axially symmetric collective oblate ($\gamma = -60°$) shape.

A negative-parity sideband based on a two-quasineutron configuration, also with a large negative γ deformation, was observed. At higher spins, this band shows a backbend caused by the alignment of a pair of $h_{11/2}$ neutrons. A second negative-parity sideband, built on a two-quasiproton configuration with a shape close to the collective prolate $\gamma = 0°$ shape, was established.

Two $\Delta I = 1$ sidebands, attributed to mixed neutron proton four-quasiparticle configurations with shapes near $\gamma = -60°$, were established. For these bands, $h_{11/2}$ neutrons drive the nucleus towards the oblate shape where high-Ω $h_{11/2}$ protons, which approach the Fermi surface, are responsible for enhanced $M1$ transitions and a lack of signature splitting in these bands.

The systematics of γ vibrational bands and quasiparticle crossing frequencies for several $N = 76$ isotones provide evidence for triaxial nuclear shapes ($\gamma \sim -30°$) at low spins in agreement with recent theoretical predictions.

ACKNOWLEDGMENTS

This work was in part supported by the National Science Foundation. The authors would like to thank T. Lauritsen for his assistance during part of the present experiments.

[1]B. D. Kern, R. L. Mlekodaj, G. A. Leander, M. O. Kortelahti, E. F. Zganjar, R. A. Braga, R. W. Fink, C. P. Perez, W. Nazarewicz, and P. B. Semmes, Phys. Rev. C **36**, 1514 (1988), and references therein.

[2]R. A. Wyss, J. Nyberg, A. Johnson, R. Bengtsson, and W. Nazarewicz, Phys. Lett. B **215**, 211 (1988).

[3]I. Ragnarsson, A. Sobiczewski, R. K. Sheline, S. E. Larsson, and B. Nerlo-Pomorska, Nucl. Phys. **A233**, 329 (1974).

[4]Y. S. Chen, S. Frauendorf, and G. A. Leander, Phys. Rev. C **28**, 2437 (1983).

[5]G. A. Leander, S. Frauendorf, and F. R. May, in *Proceedings of the Conference on High Angular Momentum Properties of Nuclei, Oak Ridge, 1982,* edited by N. R. Johnson (Harwood Academic, New York, 1983), p. 281.

[6]S. Frauendorf and F. R. May, Phys. Lett. **125B**, 245 (1983).

[7]G. Andersson, S. E. Larsson, G. Leander, P. Möller, S. G. Nilsson, I. Ragnarsson, S. Åberg, R. Bengtsson, J. Dudek, B. Nerlo-Pomorska, K. Pomorski, and Z. Szymański, Nucl. Phys. **A268**, 205 (1976).

[8]J. Hattula, S. Juutinen, M. Jaaskelainen, T. Lonnroth, A. Pakkanen, M. Piiparinen, and G. Sletten, J. Phys. G **13**, 57 (1987).

[9]W. Lieberz, S. Freund, A. Granderath, A. Gelberg, A. Dewald, R. Reinhardt, R. Wirowski, K. O. Zell, and P. von Brentano, Z. Phys. A **330**, 221 (1988).

[10]R. Reinhardt, A. Dewald, A. Gelberg, W. Lieberz, K. Schiffer, K. P. Schmittgen, K. O. Zell, and P. von Brentano, Z. Phys. A **329**, 507 (1988).

[11]R. A. Wyss, A. Johnson, F. Liden, J. Nyberg, A. H. Nelson, D. W. Banes, A. Cohen, D. J. G. Love, and J. Simpson, Proceedings of the XXV International Winter Meeting on Nuclear Physics, Bormio, 1987 (unpublished).

[12]J. P. Martin, V. Barci, H. El-Samman, A. Gizon, J. Gizon, B. M. Nyakó, W. Klamra, F. A. Beck, T. Byrski, and J. C. Merdinger, Z. Phys. A **326**, 337 (1987).

[13]K. Schiffer, A. Dewald, A. Gelberg, R. Reinhardt, K. O. Zell, Sun Xianfu, and P. von Brentano, Z. Phys. A **327**, 251 (1987).

[14]K. Schiffer, A. Dewald, A. Gelberg, R. Reinhardt, K. O. Zell, Sun Xianfu, and P. von Brentano, Nucl. Phys. **A458**, 337 (1986).

[15]Sun Xianfu, D. Bazzacco, W. Gast, A. Gelberg, U. Kaup, K. Schiffer, A. Dewald, R. Reinhardt, K. O. Zell, and P. von Brentano, Nucl. Phys. **A436**, 506 (1985).

[16]E. S. Paul, C. W. Beausang, D. B. Fossan, R. Ma, W. F. Piel, Jr., and N. Xu, Phys. Rev. C **36**, 153 (1987).

[17]E. S. Paul, S. Shi, C. W. Beausang, D. B. Fossan, R. Ma, W. F. Piel, Jr., and N. Xu, Phys. Rev. C **36**, 2380 (1987).

[18]W. Starzecki, G. De Angelis, B. Rubio, J. Styczen, K. Zuber, H. Güven, W. Urban, W. Gast, P. Kleinheinz, S. Lunardi, F. Soramel, A. Facco, C. Signorini, M. Morando, W. Meczynski, A. M. Stefanini, and G. Fortuna, Phys. Lett. B **200**, 419 (1988).

[19]R. A. Wyss, A. Johnson, J. Nyberg, R. Bengtsson, and W. Nazarewicz, Z. Phys. A **329**, 255 (1988).

[20]J. Billowes, K. P. Lieb, J. W. Noé, W. F. Piel, Jr., S. L. Rolston, G. D. Sprouse, O. C. Kistner, and F. Christancho, Phys. Rev. C **36**, 974 (1987).

[21]M. Ishii, T. Ishii, A. Makishima, and M. Ogawa, *Proceedings of the International Conference on Nuclear Physics, Harrogate, 1986* (Institute of Physics, Bristol, 1986), Vol. I, p. 45.

[22]A. Zemel, C. Broude, E. Dafni, A. Gelberg, M. B. Goldberg,

J. Gerber, G. J. Kumbartzki, and K.-H. Speidel, Nucl. Phys. **A383**, 165 (1982).
[23]R. Bengtsson and S. Frauendorf, Nucl. Phys. **A327**, 139 (1979).
[24]J. Gizon, A. Gizon, and D. J. Horen, Nucl. Phys. **A252**, 509 (1975).
[25]C. Flaum, D. Cline, A. W. Sunyar, and O. C. Kostner, Phys. Rev. Lett. **33**, 973 (1974).
[26]C. Flaum, D. Cline, A. W. Sunyar, O. C. Kistner, Y. K. Lee, and J. S. Kim, Nucl. Phys. **A264**, 291 (1976).
[27]H. Kusakari, N. Yoshikawa, H. Kawakami, M. Ishihara, Y. Shida, and M. Sakai, Nucl. Phys. **A242**, 13 (1975).
[28]A. Dewald, S. Harissopulos, G. Böhm, A. Gelberg, K. P. Schmittgen, R. Wirowski, K. O. Zell, and P. von Brentano, Phys. Rev. C **37**, 289 (1988).
[29]L. Hildingsson, C. W. Beausang, D. B. Fossan, W. F. Piel, Jr., A. P. Byrne, and G. D. Dracoulis, Nucl. Instrum. Methods A **252**, 91 (1986).
[30]G. Palameta and J. C. Waddington, Nucl. Instrum. Methods A **234**, 476 (1985).
[31]K. S. Krane, R. M. Steffen, and R. M. Wheeler, Nucl. Data Tables A **11**, 351 (1973).
[32]W. Nazarewicz, J. Dudek, R. Bengtsson, T. Bengtsson, and I. Ragnarsson, Nucl. Phys. **A435**, 397 (1985).
[33]A. Gelberg, private communication.
[34]C. J. Gallagher, Jr. and S. A. Moszkowski, Phys. Rev. **111**, 1282 (1958).
[35]R. Ma, E. S. Paul, C. W. Beausang, S. Shi, N. Xu, and D. B. Fossan, Phys. Rev. C **36**, 2322 (1987).
[36]W. F. Piel, Jr., C. W. Beausang, D. B. Fossan, L. Hildingsson, and E. S. Paul, Phys. Rev. C **35**, 959 (1987).
[37]R. Ma, K. Ahn, D. B. Fossan, Y. Liang, E. S. Paul, and N. Xu, Phys. Rev. C **39**, 530 (1989).
[38]Y. Liang, R. Ma, E. S. Paul, N. Xu, D. B. Fossan, F. Dönau, and J. Y. Zhang, Bull. Am. Phys. Soc. **34**, 1233 (1989).
[39]E. S. Paul, C. W. Beausang, D. B. Fossan, R. Ma, W. F. Piel, Jr., N. Xu, L. Hildingsson, and G. A. Leander, Phys. Rev. Lett. **58**, 984 (1987).
[40]N. Xu, C. W. Beausang, R. Ma, E. S. Paul, W. F. Piel, Jr., D. B. Fossan, and L. Hildingsson, Phys. Rev. C **39**, 1799 (1989).
[41]M. J. Godfrey, Y. He, I. Jenkins, A. Kirwan, P. J. Nolan, D. J. Thornley, S. M. Mullins, R. Wadsworth, and R. A. Wyss, J. Phys. G **15**, 671 (1989).
[42]A. S. Davydov and G. F. Filippov, Nucl. Phys. **8**, 237 (1958).
[43]*Table of Isotopes*, 7th ed., edited by C. M. Lederer and V. S. Shirley (Wiley, New York, 1978).
[44]E. S. Paul, K. Ahn, D. B. Fossan, Y. Liang, R. Ma, and N. Xu, Phys. Rev. C **39**, 153 (1989).
[45]J.-y. Zhang, private communication.
[46]S. G. Nilsson, C. F. Tsang, A. Sobiczewski, Z. Szymanski, W. Wycech, C. Gustafson, I.-L. Lamm, P. Moller, and B. Nilsson, Nucl. Phys. **A131**, 1 (1969).
[47]J.-y. Zhang, N. Xu, D. B. Fossan, Y. Liang, R. Ma, and E. S. Paul, Phys. Rev. C **39**, 714 (1989).
[48]T. Bengtsson and I. Ragnarsson, Nucl. Phys. **A436**, 14 (1985).